PROCEEDINGS A

rspa.royalsocietypublishing.org

Research

Check for updates

Article submitted to journal

Subject Areas:
Applied Mathematics, Fluid Mechanics, Wave motion

Keywords:
shallow water, metamaterial, wave scattering

Author for correspondence:
Richard Porter
e-mail: richard.porter@bristol.ac.uk

Shallow water theory for structured bathymetry

C. Marangos and R. Porter

School of Mathematics, Fry Building, Woodland Road, Bristol, BS8 1UG, UK.

A shallow water theory is developed which applies to surface wave propagation over structured bathymetry comprised of rapid abrupt fluctuations in depth between two smoothly-varying levels. Using a homogenisation approach coupled to the depth-averaging process which underpins shallow water modelling, governing equations for the wave elevation are derived which explicitly relate local spatially-varying anisotropy of wave speeds to properties of the microstructured bed.

The model is applied to two water wave scattering problems to demonstrate both the complex wave propagation characteristics exhibited by structured beds and to provide examples of how to use structured beds to engineer bespoke wave propagation. This includes propagating waves with practically zero reflection and loss of form through circular bends in channels.

1. Introduction

Linear shallow water theory is a well-established tool for predicting long-wave propagation in shallow water over variable beds. It is based on the assumption that the typical depth to lengthscale ratio, $H/L \ll 1$, whilst also requiring that the surface elevation is sufficiently small (see, for example, Stoker (1957), Whitham (1974)). Thus a rescaling of physical variables in the governing equations followed by a perturbation expansion in the small parameter $(H/L)^2$ gives, at leading order, the well-known linear shallow water equation

$$\zeta_{tt} = g\nabla \cdot (h\nabla\zeta) \tag{1.1}$$

describing the evolution of the free surface elevation $\zeta(x, y, t)$ over the variable fluid depth $h(x, y)$ subject to gravity, g. Under this description waves are non-dispersive and the wave speed is $\sqrt{gh}$.

THE ROYAL SOCIETY PUBLISHING

Recently Porter (2019) described an extension to the linear shallow water equations which includes higher-order terms at $O((H/L)^2)$ in the expansion and leads to a governing equation with the same structure as (1.1).

These equations incorporate weak dispersion and demonstrate that the wave speed is also slowed by gradients in h. As a consequence of this, it was highlighted in Porter (2019) that there can be differences in the speed of waves propagating in different directions over variable bathymetry.

The independent control of the wave speed components at every point in space is a demand often made in the design of so-called metamaterials. These are structures which interact with, and alter the propagation of, waves in a manner that is either not accessible or not encountered in conventional settings. They have been considered extensively in electromagnetics, acoustics and elasticity though less so when related to surface waves on water. Typically, the properties of a metamaterial are determined by the macroscopic effect of a microstructure whose lengthscale is significantly smaller than the lengthscale of the underlying field variable (for us, the wavelength). One of the most common features exhibited by metamaterials is negative refraction (e.g. Smith *et al.* (2004)), the ability to reverse the direction of a plane wave front as it crosses a straight interface from a conventional medium into a metamaterial. It is integral to producing exotic phenomena such as invisibility cloaking and perfect lensing (e.g. Fleury & Alú (2014), Pendry (2000)).

Whilst Porter's (2019) work shows that conventional bathymetry exhibits anisotropy of wave speeds its practical scope as a device for the bespoke manipulation of surface waves is limited by its restricted definition in terms of a single function $h(x, y)$.

Farhat *et al.* (2008) proposed the first water wave metamaterial, introduced as a device for cloaking a circular cylinder from surface waves. The cloak design involved an annular region occupied by a large periodic array of vertical posts extending uniformly through the depth but varying in cross-section radially within the annular array with a design which dictated spatially-varying and anisotropic wave speeds in the radial and angular directions. Exploiting the contrast in lengthscale between the vertical posts and the underlying wavelength, homogenisation was used to determine an effective shallow water wave equation. The coordinate transformation of space used by Farhat *et al.* (2008) required a further spatially-varying material parameter in the effective shallow water model in addition to those that introduce effective anisotropic depth effects which they did not address. Later, Zareei & Alam (2015) revisited the cylinder cloaking problem using a non-linear transformation which relaxed this additional requirement at the expense of introducing non-perfect impedance matching conditions at the edge of the cloak. Zareei & Alam (2015) showed that cloaking improved as the size of the cloak increased and as the impedance mismatch was reduced. They did not discuss a water wave metamaterial design needed in the cloak.

Closely-spaced periodic arrays of vertical cylinders were also used by Farhat *et al.* (2010) as a negative refraction lensing device for surface waves. A similar solution was used by Iida & Kashiwagi (2018) although they described their metamaterial as being comprised as a periodic network of narrow shallow vertically-walled water channels rather than a periodic array vertical posts surrounded by fluid. Their assumed geometrical configuration allowed the effective medium to be described by the exchange of wave information at junctions on the network of fluid channels between neighbouring junctions along which information propagates at the conventional shallow water wave speed.

It is also possible to control wave speeds by placing structures in the surface of the fluid (as proposed by Zareei & Alam (2016)) or on the bed of the fluid and this is where the current work is focused. In Berraquero *et al.* (2013) conventional shallow water theory was used in a standard 'layered-medium' homogenisation formulation (e.g. Mei & Vernescu (2010)) as the foundation of a design of structured bed with rapid fluctuations between two constant depths. This device was used to consider the transmission of waves through a parallel-walled waveguide containing a sharp change in direction along its length. However, conventional shallow water theory assumes small bed gradients and can only be used to determine propagation of waves over a discontinuous

change in depth in a asymptotic sense. Thus, it will only apply to structured beds when the fluctuations in the depth are no more rapid than the wavelength. In view of this Maurel *et al.* (2017) conducted a formal multiple-scales homogenisation, once again in a shallow water setting, to determine revised effective depths as solutions to a potential flow problem in a fundamental periodic cell.

More recently Maurel *et al.* (2019) have considered shallow water wave scattering by a structured bed of finite width by adopting the model of Maurel *et al.* (2017) and with a particular focus on determining effective matching conditions at the discontinuity between a conventional bed and a structured bed. This is done through a careful matched asymptotic process. At leading order matching conditions of pressure and flux are determined, as in the case of shallow water scattering by a discontinuous change in conventional bathymetry, but more sophisticated conditions are derived at the next order in the shallowness parameter, H/L.

In the current work we revisit the structured bed considered by Berraquero *et al.* (2013) and Maurel *et al.* (2017) and employ a formal multi-scale homogenisation approach under the assumption that the vertical protrusions that comprise the structured bed are closely spaced. The analysis is performed in a shallow water setting without the need to determine solutions to potential flow problems. Thus the model, developed in Section 2, determines the effective depths for waves propagating parallel and perpendicular to the structured array of barriers explicitly. The model that emerges coincides with the one proposed in Porter (2018) who use basic physical principles and conservation laws. In Section 3, we compare our expressions with the results of Berraquero *et al.* (2013) and Maurel *et al.* (2017). In Section 4, we consider scattering of waves by structured beds to both illustrate and quantify the negative refraction properties of these beds. In Section 5 we demonstrate the use of structured beds in the bespoke manipulation of waves in curved channels. The basis for this is a coordinate transformation similar to that used by Berraquero *et al.* (2013) for sharp bends in channels. The paper is summarised in Section 6.

2. Formulation of shallow water equations

(a) Description of the geometry

The theory is developed in a Cartesian framework (x, y, z) with z directed vertically upwards and $z = 0$ coinciding with the undisturbed free surface of a fluid of density ρ. The fluid is bounded below by a rigid structured bed which consists of a periodic arrangement of protrusions aligned with the y-axis of rectangular cross section and extending vertically between a lower surface described by the function $z = -h^+(x, y)$ and an upper surface given by $z = -h^-(x, y)$ such that $h^+ \geq h^-$ – see Fig. 1. Each vertical protrusion is of thickness Θl, $\Theta \in (0, 1)$, where l is the periodicity of the structure in the x-direction. The barriers are thin when $\Theta \to 0$ (we shall refer to this case as $\Theta = 0$) and the gaps close when $\Theta \to 1$. We make a close-spacing assumption implying $l/h^\pm \ll 1$.

We consider waves propagating on the surface of the fluid with amplitude $\zeta(x, y, t)$ where t is the time variable and assume that waves are of small steepness so that $|\nabla\zeta| \sim |\zeta|/\lambda \ll 1$ where λ is a characteristic wavelength (here, and in what follows, $\nabla = (\partial_x, \partial_y)$). In addition it will be assumed that $h^\pm/\lambda \ll 1$ which expresses the shallow water condition.

(b) Governing equations

The fluid is assumed to be inviscid and incompressible and its motion is represented by the velocity field $(\mathbf{u}(x, y, z, t), w(x, y, z, t))$ where $\mathbf{u} = (u, v)$ are the horizontal components of the flow. Within the fluid, mass conservation requires that

$$\nabla \cdot \mathbf{u} + w_z = 0 \tag{2.1}$$

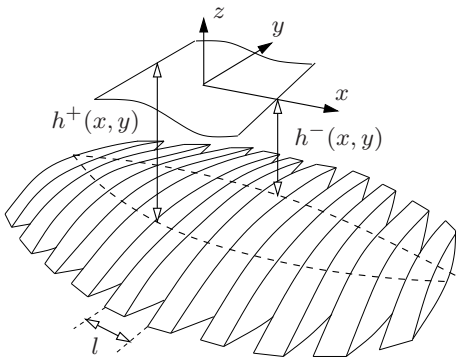

Figure 1. Illustrative sketch of a structured bed, with the horizontal (x, y) axes lying in the plane of the mean free surface.

be satisfied and momentum conservation is expressed as

$$\rho \mathbf{u}_t + \rho(\mathbf{u}\cdot\nabla + w\partial_z)\mathbf{u} = -\nabla p, \qquad \rho w_t + \rho(\mathbf{u}\cdot\nabla + w\partial_z)w = -p_z - \rho g \tag{2.2}$$

where $p = p(x, y, z, t)$ is the pressure and g is gravitational acceleration.

The kinematic and dynamic conditions on the surface of the fluid are

$$w(x, y, \zeta, t) - \mathbf{u}\cdot\nabla\zeta = \zeta_t, \qquad \text{and} \qquad p(x, y, \zeta, t) = p_a \tag{2.3}$$

where p_a is constant atmospheric pressure. Finally the no-flow conditions applied to the submerged boundary which consists of the union of a periodic arrangement of two surfaces $z = -h^+$ and $z = -h^-$ on which

$$w + \nabla h^{\pm}\cdot\mathbf{u} = 0, \qquad \text{on } z = -h^{\pm} \tag{2.4}$$

and vertical walls joining them on which

$$u_x = 0. \tag{2.5}$$

(c) Non-dimensionalisation

There are four lengthscales in the problem: (i) L is a characteristic horizontal lengthscale either representing the underlying wavelength or the scale over which macroscopic changes to the fluid depth occur; (ii) H is a characteristic depth of fluid; (iii) l is the lengthscale of the structured bed; (iv) A is a characteristic wave height.

We form three dimensionless quantities from these parameters:

$$\mu = H/L, \qquad \epsilon = l/L, \qquad \text{and} \qquad \delta = A/H \tag{2.6}$$

which represent, respectively, shallowness, microstructure contrast and linearisation (wave steepness) parameters. Each one is supposed to be small and we demand the theory to work in the limit $\delta \to 0$ independently of the size of ϵ and μ. This ensures we operate within in a linearised setting. These other two parameters are coupled by the geometry and we assume that that $\epsilon = O(\mu^2)$.

In the definition of dimensionless variables, we also take into account the two distinct lengthscales in the x-direction to perform a multiple scales expansion in x. Thus, we write

$$x = lX' + Lx', \qquad y = Ly', \qquad z = Hz', \qquad \zeta = A\zeta' \tag{2.7}$$

and accordingly $h = Hh'$ for $h = h^{\pm}$. Then we select a timescale, $T = L/\sqrt{gH}$ based on the shallow water dispersion relation so that $t = (L/\sqrt{gH})t'$ whilst the characteristic vertical velocity

scale is set by A/T so we write

$$w = (A/L)\sqrt{gH}w' \qquad \text{while} \qquad \mathbf{u} = (A/H)\sqrt{gH}\mathbf{u}' \tag{2.8}$$

is set by requiring a balance of terms at leading order in the continuity equation. Finally, the pressure references the background pressure with $p = \rho g H p'$. Under the transformation above the governing equations read

$$\nabla' \cdot \mathbf{u}' + w'_{z'} + \frac{1}{\epsilon}u'_{X'} = 0 \tag{2.9}$$

where $\nabla' = (\partial_{x'}, \partial_{y'})$ with

$$\delta u'_{t'} = -\frac{1}{\epsilon}p'_{X'} - p'_{x'}, \qquad \delta v'_{t'} = -p'_{y'}, \qquad \delta\mu^2 w'_{t'} = -p'_{z'} - 1, \tag{2.10}$$

neglecting the non-linear terms in the momentum equation since they are $O(\delta^2)$, with boundary conditions

$$w' = \zeta'_{t'}, \qquad p' = p'_a \tag{2.11}$$

on $z' = \delta\zeta'$ and, for now, we abbreviate the set of conditions on the fixed submerged bed as $(\mathbf{u}', w') \cdot \hat{\mathbf{n}} = 0$ where $\hat{\mathbf{n}}$ is normal to the bed.

(d) Expansion

We drop the primes from the dimensionless variables and expand the unknowns as

$$p \approx p^{(0)}(x, y, z, t; X) + \delta(p^{(1)} + \epsilon p^{(2)} + \ldots) \tag{2.12}$$

with

$$u \approx u^{(1)} + \epsilon u^{(2)} + \ldots, \qquad v \approx v^{(1)} + \epsilon v^{(2)} + \ldots, \qquad w \approx w^{(1)} + \epsilon w^{(2)} + \ldots \tag{2.13}$$

in which all functions, not just $p^{(0)}$, are presumed to depend upon the variables x, y, z, t, X. These expansions will be valid away from the interface $z = -h^-(x, y)$ around which local effects will require a rescaling of coordinates. Additionally, we write

$$\zeta \approx \zeta^{(1)}(x, y, t; X) + \epsilon\zeta^{(2)}(x, y, t; X) + \ldots. \tag{2.14}$$

The expansion of variables in δ is limited to capture only terms up to and including $O(\delta)$ consistent with linearisation of the momentum equations. Then (2.9) becomes

$$\frac{1}{\epsilon}u^{(1)}_X + \nabla \cdot \mathbf{u}^{(1)} + w^{(1)}_z + u^{(2)}_X + O(\epsilon) = 0 \tag{2.15}$$

and three equations in (2.10) become

$$\frac{1}{\epsilon}p^{(0)}_X + p^{(0)}_x + \delta\left(\frac{1}{\epsilon}p^{(1)}_X + u^{(1)}_t + p^{(1)}_x + p^{(2)}_X + O(\epsilon)\right) = 0 \tag{2.16}$$

with

$$p^{(0)}_y + \delta\big(v^{(1)}_t + p^{(1)}_y + O(\epsilon)\big) = 0 \tag{2.17}$$

and

$$p^{(0)}_z + 1 + \delta\big(p^{(1)}_z + O(\epsilon)\big) = 0. \tag{2.18}$$

In the last of these, the assumption that $\mu^2 = O(\epsilon)$ has been used. The dynamic boundary condition is expanded, neglecting $O(\delta^2)$ terms, to give

$$p_a = p^{(0)} + \delta\big(\zeta^{(1)}p^{(0)}_z + p^{(1)} + O(\epsilon)\big), \qquad \text{on } z = 0 \tag{2.19}$$

whilst the kinematic boundary condition is

$$w^{(1)} = \zeta_t^{(1)}, \qquad \text{on } z = 0 \tag{2.20}$$

to leading order. No-flow conditions on the surfaces of the structured bathymetry include

$$\begin{cases} w^{(n)} + \nabla h^- \cdot \mathbf{u}^{(n)} = 0, & z = -h^-,\ 0 < X < \Theta, \\ w^{(n)} + \nabla h^+ \cdot \mathbf{u}^{(n)} = 0, & z = -h^+,\ \Theta < X < 1, \\ u_X^{(n)} = 0, & -h^+ < z < -h^-,\ X = \Theta, 1 \end{cases} \tag{2.21}$$

for $n = 1, 2, \ldots$.

From (2.18) and from (2.16), (2.17) and (2.19) we have

$$p^{(0)} = p_a - z \tag{2.22}$$

which is just the background hydrostatic pressure in the fluid.

From the $O(\epsilon^{-1})$ terms in (2.15), (2.16) we have that $u^{(1)} = u^{(1)}(x, y, z, t)$ and $p^{(1)} = p^{(1)}(x, y, z, t)$ are both independent of the microscale coordinate X. Then from (2.18) with (2.19) we have $p_z^{(1)} = 0$ and $p^{(1)} = -\zeta^{(1)} p_z^{(0)}$ on $z = 0$ so that

$$p^{(1)} = \zeta^{(1)}(x, y, t). \tag{2.23}$$

We also have $v_t^{(1)} = -p_y^{(1)}$ which means that

$$v_t^{(1)} = -\zeta_y^{(1)} \tag{2.24}$$

and $v^{(1)} = v^{(1)}(x, y, t)$ is therefore independent of both z and X.

We can also see that first order variables are defined by

$$\nabla \cdot \mathbf{u}^{(1)} + w_z^{(1)} = -u_X^{(2)} \tag{2.25}$$

with

$$u_t^{(1)} + p_x^{(1)} = -p_X^{(2)} \tag{2.26}$$

in terms of higher-order quantities. In $-h^- < z < 0$ above the structured bed where the fluid is continuous we use the multiple-scales assumption that $p^{(2)}$ is a periodic function of X and since the left-hand side of (2.26) has been shown to be independent of X we can integrate over a period, $0 < X < 1$, to give

$$u_t^{(1)} = -\zeta_x^{(1)} \tag{2.27}$$

after use of (2.23). Combining with (2.24) implies

$$\mathbf{u}_t^{(1)} = -\nabla \zeta^{(1)} \tag{2.28}$$

in $-h^- < z < 0$. Thus $u^{(1)} = u^{(1)}(x, y, t)$ only.

Returning to (2.25), $u^{(2)}$ is periodic in X for $-h^- < z < 0$ and integrating from $0 < X < 1$ gives

$$u_x^{(1)} + v_y^{(1)} + \int_0^1 w_z^{(1)}\, dX = 0. \tag{2.29}$$

Integrating over $-h^- < z < 0$ gives

$$\begin{aligned} h^-(u_x^{(1)} + v_y^{(1)}) &= -\int_0^1 w^{(1)}|_{z=0} - w^{(1)}|_{z=-h^-+0}\, dX \\ &= -\zeta_t^{(1)} - \nabla h^- \cdot \mathbf{u}^{(1)} + \int_0^1 \left(w^{(1)} + \nabla h^- \cdot \mathbf{u}^{(1)} \right)_{z=-h^-+0} dX \end{aligned} \tag{2.30}$$

after using (2.20) and the first boundary condition in (2.21) with $n = 1$. We note that although equations above have been stated as applying through $-h^- < z < 0$, formally they apply away

from the boundary $z=-h^-$ where local effects due the flow transition from the fluid above the interface to the fluid in the channels below should be taken into account. A matched asymptotic expansion scheme is the formal manner in which this interface can be addressed and in (2.30) the evaluation is made at $z=-h^-+0$ indicating that this is the inner limit of the outer solution in z far away from h^-. We access the inner matching region with a rescaling of the vertical coordinate defined by $z=-h^-(x,y)+\epsilon Z$. Under this rescaling, the dominant contributions from (2.15) to (2.18) are in the form

$$u_X^{(1)}+w_Z^{(1)}=0, \qquad p_X^{(1)}=p_Z^{(1)}=0. \tag{2.31}$$

Therefore, in this inner region $p^{(1)}=p^{(1)}(x,y,t)$ does not depend on the local spatial coordinates X, Z. Leading order matching to the regions above and below $z=-h^-$ implies the leading order hydrodynamic pressure variation in $z<-h^-$ is also $p^{(1)}(x,y,t)$ (i.e. there is no jump in pressure across the interface between the microstructure and the fluid above). In turn, from (2.17) and (2.23) we have

$$v_t^{(1)}=-p_y^{(1)}=-\zeta_y^{(1)}, \qquad \text{in } -h^+<z<-h^- \tag{2.32}$$

is unchanged from the region $-h^-<z<0$ and $v^{(1)}=v^{(1)}(x,y,t)$ in the fluid in the narrow gaps. Next, we use the fact that $v^{(1)}$ does not depend on a local scale Y and integrate the first equation in (2.31) over a local cell volume $D=\{0<X,Y<1,\ 0<Z<Z^*\}\cup\{\Theta<X<1,\ 0<Y<1,\ -Z^*<Z<0\}$ to give, using the divergence theorem,

$$0=\int_D (u_X^{(1)}+v_Y^{(1)}+w_Z^{(1)})\,dX\,dY\,dZ=\int_{\partial D}(u^{(1)},v^{(1)},w^{(1)})\cdot\hat{\mathbf{n}}\,dS \tag{2.33}$$

and $\hat{\mathbf{n}}$ points out of D. Using the periodicity of $u^{(1)}$ across $X=0,1$ in $Z>0$, the local Neumann conditions expressed by (2.21) and the independence in Y of $v^{(1)}$ and implies that

$$\int_0^1(\mathbf{u}^{(1)},w^{(1)})\cdot\hat{\mathbf{n}}|_{Z=Z^*}\,dX+\int_\Theta^1(\mathbf{u}^{(1)},w^{(1)})\cdot\hat{\mathbf{n}}|_{Z=-Z^*}\,dX=0. \tag{2.34}$$

Asymptotic matching implies the inner limit of the incoming flux from the outer solution away from the interface matches the outer limit ($Z^*\to\infty$) of the flux in the inner solution in (2.30). That is to say,

$$\int_0^1\left(w^{(1)}+\nabla h^-\cdot\mathbf{u}^{(1)}\right)_{z=-h^-+0}dX=\int_\Theta^1\left(w^{(1)}+\nabla h^-\cdot\mathbf{u}^{(1)}\right)_{z=-h^--0}dX. \tag{2.35}$$

Away from the interface in $-h^+<z<-h^-$, the equation (2.15) at leading order gives us $u_X^{(1)}=0$ and, with the last boundary condition in (2.21), $n=1$, we have $u^{(1)}=0$, whilst at the next order $v_y^{(1)}+w_z^{(1)}=-u_X^{(2)}$ holds for $\Theta<X<1$. We integrate over this interval using (2.21) again with $n=2$, to give

$$(1-\Theta)v_y^{(1)}+\int_\Theta^1 w_z^{(1)}\,dX=0 \tag{2.36}$$

after using the independence from X and z of $v^{(1)}$ in the channels and integrating this over the depth $-h^+<z<-h^-$ gives

$$\begin{aligned}(h^+-h^-)(1-\Theta)v_y^{(1)}&=-\int_\Theta^1 w^{(1)}|_{z=-h^--0}-w^{(1)}|_{z=-h^+}\,dX\\&=-(1-\Theta)h_y^+v^{(1)}+(1-\Theta)h_y^-v^{(1)}-\int_\Theta^1\left(w^{(1)}+h_y^-v^{(1)}\right)_{z=-h^--0}dX\end{aligned} \tag{2.37}$$

after using (2.21) and the fact that $u^{(1)}=0$ in the channels.

We can now use (2.30) and (2.37) in the asymptotic matching condition (2.35) and this results in

$$\zeta_t^{(1)} + (h^- u^{(1)})_x + \left(\Theta h^- + (1-\Theta)h^+)v^{(1)}\right)_y = 0 \tag{2.38}$$

or, more compactly,

$$\zeta_t^{(1)} + \nabla \cdot \mathsf{h}\mathbf{u}^{(1)} = 0 \tag{2.39}$$

where

$$\mathsf{h} = \begin{pmatrix} h^- & 0 \\ 0 & \bar{h} \end{pmatrix}, \qquad \bar{h} = \Theta h^- + (1-\Theta)h^+ \tag{2.40}$$

in tensorial form. It is more natural to use, in place of $\mathbf{u}^{(1)}$, the quantity

$$\mathbf{q}^{(1)} = \mathsf{h}\mathbf{u}^{(1)} \tag{2.41}$$

since this represents the horizontal flux of fluid and then (2.39) is just

$$\zeta_t^{(1)} = -\nabla \cdot \mathbf{q}^{(1)} \tag{2.42}$$

which is presented in the form of a standard conservation law that one might have arrived at using physical principles without any detailed asymptotic analysis (as in Porter (2018)).

This leading order theory is completed by cell-integrating the horizontal momentum equations established in (2.28) and (2.32) above and below the interface $z = -h^-$ so that

$$\mathbf{0} = \int_0^1 \int_{-h^-}^0 \left(\mathbf{u}_t^{(1)} + \nabla\zeta^{(1)}\right) dz\, dX + \int_\Theta^1 \int_{-h^+}^{-h^-} \left(v_t^{(1)} + \zeta_y^{(1)}\right)\hat{\mathbf{y}}\, dz\, dX \tag{2.43}$$

all quantities being independent of X and z and this provides us with

$$\mathbf{q}_t^{(1)} = -\mathsf{h}\nabla\zeta^{(1)}. \tag{2.44}$$

Finally, we can eliminate between (2.42) and (2.44) to get either

$$\zeta_{tt}^{(1)} = \nabla \cdot (\mathsf{h}\nabla\zeta^{(1)}) \tag{2.45}$$

or

$$\mathbf{q}_{tt}^{(1)} = \mathsf{h}\nabla(\nabla \cdot \mathbf{q}^{(1)}). \tag{2.46}$$

Returning to dimensional variables with $\zeta(x,y,t) \approx \zeta^{(1)}(x,y,t)$ introduces a factor of g into the right-hand side of (2.44) and (2.45) reads

$$\zeta_{tt} = g\nabla \cdot (\mathsf{h}\nabla\zeta) \tag{2.47}$$

which is the extension of (1.1) for structured bathymetry.

3. Comparison with other models

As indicated in the Introduction, the shallow water equation developed in Section 2 is not the only model that has been developed for wave propagation over structured bathymetry.

Previously, Berraquero *et al.* (2013) and Maurel *et al.* (2017) have presented methods for determining the effective depth component in the tensor $\mathsf{h} = \mathrm{diag}\{h_1, h_2\}$ in a shallow water setting. In both these models, a value of $h_2 = \Theta h^- + (1-\Theta)h^+$ is deduced and coincides with the expression of $\bar{h}$ derived in Section 2. There are differences between the models in the definition of h_1. The shallow water model of Berraquero *et al.* (2013) sets

$$h_1 = 1/(\Theta/h^- + (1-\Theta)/h^+) \tag{3.1}$$

which tends to h^- when $\Theta \to 1$ and h^+ when $\Theta \to 0$. This contrasts with the constant value of $h_1 = h^+$ deduced in Section 2. For reasons described in the Introduction, we expect the model

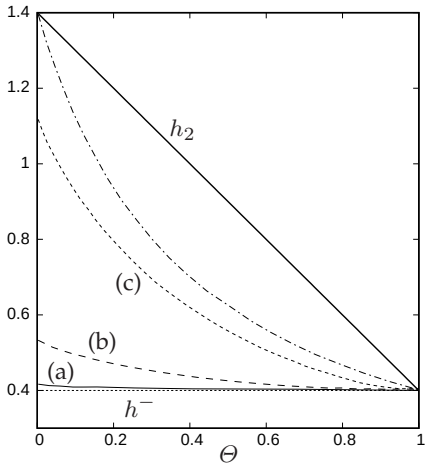

Figure 2. Reproduction of Fig. 8 (a) from Maurel *et al.* (2017) for $h^+ = 1.4$, $h^- = 0.4$, measuring the variation of effective depths h_1 and h_2 as a function of Θ: $h_2 = h^-\Theta + (1-\Theta)h^+$ (solid line) is common too all models; $h_1 = 1/(\Theta/h^- + (1-\Theta)/h^+)$ (chained) the Berraquero *et al.* (2013) model; $h_1 = h^-$ (our model); and computations for: (a) $l/h^+ = 0.04$, (b) $l/h^+ = 0.4$, (c) $l/h^+ = 4$.

of Berraquero *et al.* (2013) to work for protrusions which are widely-spaced (on the scale of the wavelength, or $l/h^+ \gg 1$) whilst we have assumed the opposite limit that protrusions are closely-spaced, or $l/h^+ \ll 1$.

Spanning these two limiting cases is the numerically-determined value proposed by the Maurel *et al.* (2017) model which arises through a formal homogenisation of the governing equations, following the methodology introduced by Rosales & Papanicolaou (1983). This was performed under a shallow water assumption without assumptions on the size of l/h^+ but requires the full depth-dependent potential theory description. Maurel *et al.* (2017) provide the details to determine the value of h_1 numerically and then compare, in their Fig. 8(a) (and reproduced here in Fig. 2), the values of h_1 from this method against the value of h_1 given by (3.1) from the effective shallow water model of Berraquero *et al.* (2013) as the thickness parameter Θ varies for three different values of l/h^+.

As l/h^+ increases the computed values of h_1 tend slowly to the wide-spacing shallow water model of Berraquero *et al.* (2013), as we have argued for above. As l/h^+ decreases their results converge quite rapidly to the constant value of $h_1 = h^-$ which is the result from our effective shallow water model. As Maurel *et al.* (2017) discuss, it is this closely-spaced arrangement with $\Theta = 0$ which gives rise to the largest contrast between h_1 and h_2 and hence the greatest anisotropy in propagating wave speeds.

4. Analysis of wave transmission across structured beds

We assess the basic characteristics of the structured metamaterial bed by considering the propagation of plane waves from a constant depth h_0 in $x < 0$ obliquely incident on a metamaterial bed in $x > 0$ having constant values of h^+, h^- and Θ. We also allow the structured bed in $x > 0$ to be rotated through an anticlockwise angle δ as illustrated in Fig. 3.

In other words (1.1) holds in $x < 0$ whilst (2.42), (2.44) hold for functions $\tilde{\zeta}(\tilde{x}, \tilde{y}, t)$ and $\tilde{\mathbf{q}}(\tilde{x}, \tilde{y}, t)$ in a coordinate system $(\tilde{x}, \tilde{y})$ rotated by δ from (x, y). That is

$$\begin{pmatrix} \tilde{x} \\ \tilde{y} \end{pmatrix} = \mathcal{R} \begin{pmatrix} x \\ y \end{pmatrix}, \qquad \text{where} \qquad \mathcal{R} = \begin{pmatrix} \cos\delta & \sin\delta \\ -\sin\delta & \cos\delta \end{pmatrix}. \tag{4.1}$$

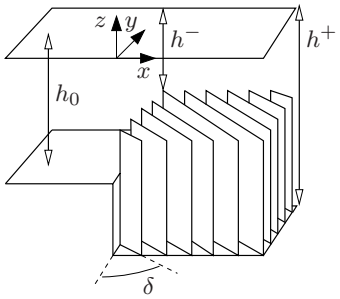

Figure 3. Sketch of transition from a constant depth in $x<0$ to a structured bed in $x>0$. The diagram indicates thin barriers where $\Theta=0$.

Making the change of variables from $(\tilde{x},\tilde{y})$ aligned with the structure to (x,y) in $x>0$ we have

$$\zeta_t=-\nabla\cdot\mathbf{q}, \qquad \text{and} \qquad \mathbf{q}_t=-g\mathcal{R}^T\mathsf{h}\mathcal{R}\nabla\zeta \tag{4.2}$$

and we let

$$\mathsf{h}_\delta=\mathcal{R}^T\mathsf{h}\mathcal{R}=\begin{pmatrix}\mathsf{h}_{11} & \mathsf{h}_{12}\\ \mathsf{h}_{12} & \mathsf{h}_{22}\end{pmatrix} \tag{4.3}$$

whose elements are defined by

$$\mathsf{h}_{11}=h^-\cos^2\delta+\bar{h}\sin^2\delta, \qquad \mathsf{h}_{12}=(h^--\bar{h})\cos\delta\sin\delta, \qquad \mathsf{h}_{22}=\bar{h}\cos^2\delta+h^-\sin^2\delta. \tag{4.4}$$

The governing equation for ζ is now

$$\zeta_{tt}=g\nabla\cdot(\mathsf{h}_\delta\nabla\zeta). \tag{4.5}$$

Assuming time-harmonic motion of angular frequency ω so that $\zeta=\Re\{\eta(x,y)\mathrm{e}^{-\mathrm{i}\omega t}\}$, the general solution of (1.1) in $x<0$ due to a plane wave incident from minus infinity propagating at an angle θ_0 with respect to the x-axis is

$$\eta(x,y)=(\mathrm{e}^{\mathrm{i}\alpha_0 x}+R\mathrm{e}^{-\mathrm{i}\alpha_0 x})\mathrm{e}^{\mathrm{i}\beta_0 y} \tag{4.6}$$

where R is the reflection coefficient, $\alpha_0=k_0\cos\theta_0$, $\beta_0=k_0\sin\theta_0$ and $k_0^2=\omega^2/gh_0$ defines the wavenumber.

The general solution of (4.5) in $x>0$ which inherits the variation of η in y from $x<0$ and satisfies a radiation condition at infinity is

$$\eta(x,y)=T\mathrm{e}^{\mathrm{i}\alpha_1^+ x}\mathrm{e}^{\mathrm{i}\beta_0 y} \tag{4.7}$$

where T is the transmission coefficient and α_1^+ is determined from the governing equation (4.5) by

$$\alpha_1^\pm=\frac{-\mathsf{h}_{12}\beta_0\pm\sqrt{\mathsf{h}_{12}^2\beta_0^2+\mathsf{h}_{11}(k_0^2h_0-\beta_0^2\mathsf{h}_{22})}}{\mathsf{h}_{11}} \tag{4.8}$$

where $\omega^2/g=k_0^2h_0$ has been used. We will discuss the nature of the roots of this equation and how this relates to the previously stated radiation condition being satisfied in a moment. For now, the solution is completed by imposing matching conditions at $x=0$. Formally this needs to be done asymptotically since both conventional and structured bed shallow water models do not apply in the vicinity of discontinuities in properties of the bed. We face a similar issue to the one encountered in the derivation of the model in Section 2 across the level $z=-h^-$. At leading order, a local scaling of the coordinate system reveals that the pressure depends only on a macroscale coordinates and the consequence of this is that η is continuous across $x=0$. The second condition that arises at leading order in the asymptotic matching is that the depth

averaged flux is continuous across $x=0$. These leading-order matching conditions, as well as higher-order conditions, have been determined by Maurel *et al.* (2019) and Marigo & Maurel (2017) for two particular configurations. The adoption of higher-order conditions in the matching at $x=0$ would be inconsistent with the use of the shallow water model over the structured bed which has neglected them. Thus the first condition $\eta(0^-,y)=\eta(0^+,y)$ gives us

$$1+R=T \tag{4.9}$$

and the flux condition is expressed as $h_0\eta_x(0^-,y)=\hat{\mathbf{x}}\cdot\mathsf{h}_\delta\nabla\eta(0^+,y)$ which results in

$$\alpha_0 h_0(1-R)=T(\alpha_1^+\mathsf{h}_{11}+\beta_0\mathsf{h}_{12}). \tag{4.10}$$

Eliminating between (4.9) and (4.10) gives

$$R=\frac{\cos\theta_0-Q}{\cos\theta_0+Q},\qquad T=\frac{2\cos\theta_0}{\cos\theta_0+Q} \tag{4.11}$$

where

$$Q = (k_0h_0)^{-1}\sqrt{\mathsf{h}_{12}^2\beta_0^2+\mathsf{h}_{11}(k_0^2h_0-\beta_0^2\mathsf{h}_{22})} \tag{4.12}$$

$$= \sqrt{(\mathsf{h}_{12}/h_0)^2\sin^2\theta_0+(\mathsf{h}_{11}/h_0)(1-(\mathsf{h}_{22}/h_0)\sin^2\theta_0)}. \tag{4.13}$$

after $\beta_0=k_0\sin\theta_0$ is used. Note that R and T are independent of k_0; it is typical of leading-order shallow water theory that scattering is purely geometric. In fact for wave scattering over a step change in water depth of conventional bathymetry, the adoption of a higher-order matching condition introduces a dependence on k_0 which only affects the phase of R but not $|R|$ (see Mei (1983)). Note also that R and T are symmetric in θ_0, the incident wave angle, and δ, the rotation of the structured bed. These are also features of the related work of Porter (2021) on refraction of water waves by plate arrays extending through the depth over a flat bed.

We return to (4.8) where there are three distinct cases to consider. The first is that $k_0^2h_0-\beta_0^2\mathsf{h}_{22}>0$ from which it follows that Q and α_1^+ are real and $\alpha_1^+>0$. This therefore holds when

$$\sin^2\theta_0<h_0/(\bar{h}\cos^2\delta+h^-\sin^2\delta), \tag{4.14}$$

a condition which is guaranteed to hold if h^+ and h^- are both less than h_0.

The second case is that $k_0^2h_0-\beta_0^2\mathsf{h}_{22}\le 0$ but Q and hence α_1^+ remains real. In this case $\alpha_1^+\le 0$ which implies from (4.7) that x-component of the phase speed of the transmitted wave is negative. Whilst this seems counterintuitive, the radiation condition at infinity is satisfied since this requires that the flux of energy is directed away from $x=0$. Thus, rearranging (4.8) for ω, the group velocity is

$$\mathbf{c}_g=\left(\frac{\partial\omega}{\partial\alpha_1^+},\frac{\partial\omega}{\partial\beta_0}\right)=(g/\omega)(k_0h_0Q,\beta_0\mathsf{h}_{22}+\alpha_1^+\mathsf{h}_{12}) \tag{4.15}$$

and the x-component is positive, as required.

In the third case $\mathsf{h}_{12}^2\beta_0^2+\mathsf{h}_{11}(k_0^2h_0-\beta_0^2\mathsf{h}_{22})<0$ and now $Q=\mathrm{i}P$, $P>0$, to ensure that $\eta\to 0$ as $x\to\infty$. It follows from (4.11) that $|R|=1$ whilst T represents the amplitude of what is now an evanescent wave field in $x>0$. As in the second case, this can only happen if the bed depth h^+ in $x>0$ is greater than h_0 in $x<0$ and is analogous to total internal reflection of oblique waves travelling from shallow water into deeper water over conventional bathymetry.

Figs. 4(a),(b) show $|R|$ as a function incident wave angle θ_0 for wave reflection by a structured bed in $x>0$ having a raised protrusions $h_0/h^-=2$ from a sunken bed at $h^+/h_0=2$. For the purposes of comparison, in the figures the short-dashed lines represent the variation of $|R|$ for a conventional/unstructured raised bed in $x>0$ ($h_0/h^-=2$) and the long-dashed line a conventional/unstructured sunken bed in $x>0$ ($h^+/h_0=2$) exhibiting total internal reflection for $|\theta_0|>45^\circ$. These two values are equal for normal incidence ($\theta_0=0$) and given by a value of $(\sqrt{2}-1)/(\sqrt{2}+1)\approx 0.17$. The sequence of solid curves show the effect of the width of the

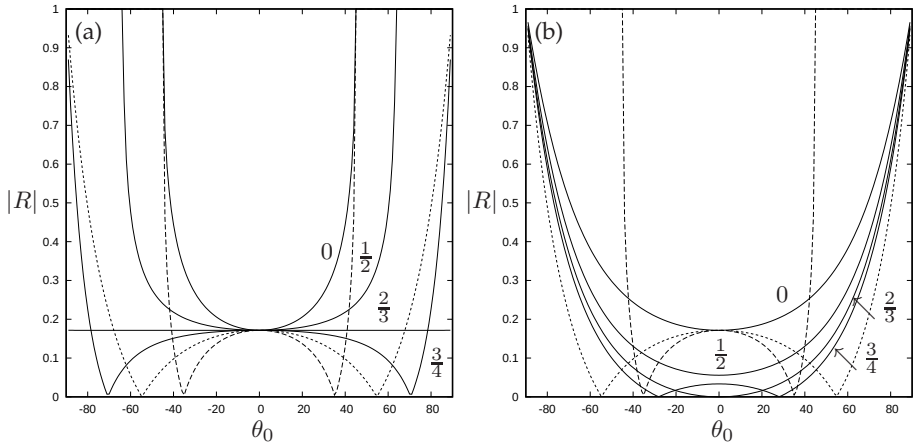

Figure 4. Modulus of reflection coefficient as a function of incident wave angle θ_0 for a structured bed in $x>0$ with $h_0/h^-=2$, $h^+/h_0=2$ for $\Theta=0,\ \frac{1}{2},\ \frac{2}{3},\ \frac{3}{4}$ (shown against solid curves) and: (a) $\delta=0^\circ$; (b) $\delta=90^\circ$.

protrusions, through the variation of Θ on reflection. In each figure $\Theta\to 1$ approaches scattering by a conventional raised bed as the gaps between the protrusions are cut-off.

In Fig. 4(a) the protrusions in the structured bathymetry are aligned with the y-axis and the variation of $|R|$ with θ_0 is quite significantly affected by the thickness of the protrusions compared to Fig. 4(b) where the protrusions are aligned with the x-axis. Of particular note is the value of $\Theta=\frac{2}{3}$ in Fig. 4(a) which shows that $|R|$ is independent of θ_0. This can be understood by considering (4.11) with (4.13) and noting that Q is proportional to $\cos\theta_0$ provided

$$h_0=\mathsf{h}_{22}-\mathsf{h}_{12}^2/\mathsf{h}_{11} \tag{4.16}$$

resulting in

$$R=(\sqrt{h_0}-\sqrt{\mathsf{h}_{11}})/(\sqrt{h_0}+\sqrt{\mathsf{h}_{11}}). \tag{4.17}$$

There is nothing special about the parameters used to produce Fig. 4(a) and there are many configurations for which (4.16) holds and $|R|$ is independent of θ_0. In particular, it is possible to find parameters for which $\mathsf{h}_{11}=h_0$ in addition to (4.16) being satisfied, implying that $R=0$ for all incident wave angles θ_0 (in addition to all wavenumbers k_0) ! Thus, we require

$$\bar{h}/h_0=(1\pm\sqrt{1-4\sin^2\delta\cos^2\delta})/(2\sin^2\delta),\qquad h^-=(1-\bar{h}\sin^2\delta)/\cos^2\delta. \tag{4.18}$$

For example, with $\Theta=0$, $\delta=30^\circ$ this perfect transparency be achieved with $h_0/h^-=3$, $\bar{h}/h_0=3$. This device could be used as a bathymetric lens with refractive characteristics defined by Fig. 6.

In addition to determining R and T we are interested how waves propagate into $x>0$ and assign the angle θ_1 to the direction in which energy propagates, or the direction of $\mathbf{c}_g$ in (4.15), This also coincides with the direction of the flux vector but is, in general, for structured beds not aligned to the phase velocity as we have already suggested and as later figures will illustrate.

In Fig. 5 the direction of energy propagation over the structured bed, θ_1, is plotted as a function of incident angle, θ_0, for thin protruding thin barriers ($\Theta=0$) rotated through $\delta=45^\circ$. In Fig. 5(a) we have set the lower level of the structured bed at the depth in $x<0$ ($h^+=h_0$) and varied the height of the protruding thin barriers, h_0/h^-, from 2 to 8. Obviously, when $h_0/h^-=1$ there is just a flat bed in $x>0$ of depth h_0 and no scattering (represented in the plot by the dotted line $\theta_1=\theta_0$). When $\theta_0=-45^\circ$ the incident waves pass uninterrupted between the thin barriers and so $\theta_1=-45^\circ$ for all h_0/h^-. As h_0/h^- increases, the thin plates in the structured bed approach the surface and the curves tend towards $\theta_1=-45^\circ$ (dotted line) for all θ_0, coinciding with the limiting case considered in Porter (2021) in which the barriers extend throughout the depth. Negative refraction occurs whenever θ_0 and θ_1 are different signs. For $h_0/h^-\gtrsim 4$ negative refraction occurs across all

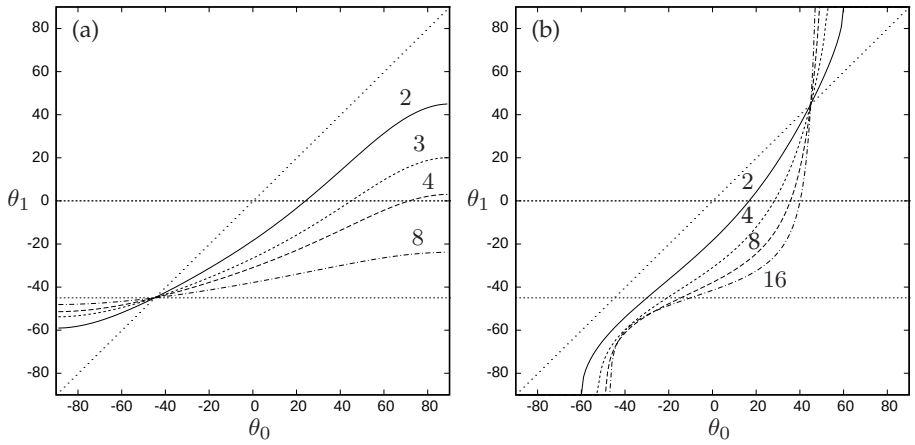

Figure 5. The variation of wave propagation, θ_1, over the structured bed due to an incident wave of angle θ_0 for $\delta = 45°$, $\Theta = 0$: (a) $h^+/h_0 = 1$ and $h_0/h^- = 2, 3, 4, 8$; (b) $h_0/h^- = 1$ and $h^+/h_0 = 2, 4, 8, 16$.

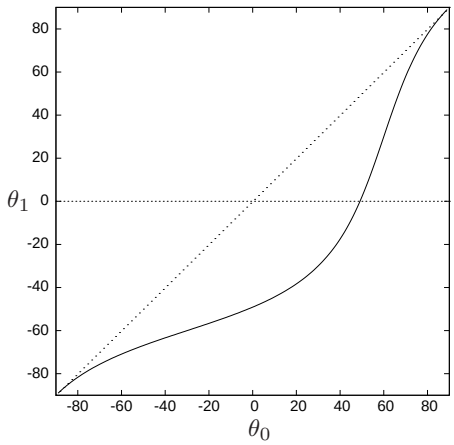

Figure 6. The variation of wave propagation, θ_1, over the structured bed due to an incident wave of angle θ_0 for an all-angle/all-frequency perfectly transmission parameters $\delta = 30°$, $\Theta = 0$, $h^+/h_0 = 3$ and $h_0/h^- = 3$.

incident wave angles and for $h_0/h^- \lesssim 4$ negative refraction is restricted to a range of incident angles. In Fig. 5(b), the top of the thin barriers are set at the depth in $x < 0$ ($h_0/h^- = 1$) and the depth of troughs between the barriers, h^+/h_0 is varied from 2 to 16. Obviously for $h^+/h_0 = 1$ we have a flat bed at a depth h_0 in $x > 0$ and there is no scattering (dotted line $\theta_1 = \theta_0$). When $\theta_0 = 45°$ the waves pass over the depth $h^- = h_0$ without scattering and so all curves pass through $\theta_1 = 45°$. The principle difference between Figs. 5(a),(b) is the onset of total internal reflection for waves travelling into structured beds with a sunken component for incident waves that are sufficiently oblique. We see that as h^+/h_0 increases the structured bed in $x > 0$ has thin barriers occupying an increasing proportion of the fluid depth and the results tend towards $\theta_1 = -45°$ again as in Fig. 5(a). In this example, negative refraction is exhibited when the incident wave angle lies between $0°$ and $45°$.

Surface plots of refracted wave fields are presented as part of the sectionthat follows. What is evident from these plots is that solutions being discussed here can also be interpreted as wave propagation in parallel-walled channels with walls in $x < 0$ angled at θ_0 and at θ_1 in $x > 0$, joined at $x = 0$ through a sharp bend. This is therefore a generalisation of the analysis of Berraquero *et*

al. (2013) who considered the specific case of a channel in $x<0$ with $\theta_0=0$. Their work used a coordinate transformation to map a straight uniform waveguide into a bent waveguide which introduced an anisotropic effective depth tensor h related to the mapping angle θ_1 and was designed to be reflectionless. Those symmetric tensor elements were equated to the symmetric tensor h_δ for a rotated structured bed having constant properties, Θ, h^- and h^+, exactly as described here and this provided three equations for the three independent parameters, h^-, $\bar{h}$ and δ (in the notation of Berraquero *et al.* (2013) $h_\parallel$, $h_\perp$ and α). This allowed them to design experiments to test the theory.

We can recreate Berraquero *et al.* (2013)'s device by setting $\theta_0=0$ and defining θ_1, the direction of the the flux vector, aligned to $\mathbf{c}_g$, and to the walls of the bent section of the waveguide in $x>0$ by

$$\tan\theta_1=\mathsf{h}_{12}/h_0, \qquad \text{and} \qquad \mathsf{h}_{11}=h_0 \tag{4.19}$$

from requiring $R=0$ from (4.17). This specifies just two conditions for the three independent parameters which can be expressed alternatively as

$$h^-/h_0=1+\tan\theta_1\tan\delta, \qquad \text{and} \qquad \bar{h}/h_0=1-\tan\theta_1/\tan\delta. \tag{4.20}$$

That is, there is not a unique configuration as suggested by Berraquero *et al.* (2013)'s analysis. For example, with $\theta_1=30^\circ$ we can choose $\delta=-45^\circ$ upon which $h^-/h_0=1-1/\sqrt{3}$ and $\bar{h}/h_0=1+1/\sqrt{3}$; but δ can take other values (see the paragraph below). The additional constraint of Berraquero *et al.* (2013), which can be confirmed by comparing their analysis to ours, is the satisfaction of the equivalent of our (4.16) implying that their structured waveguide in $x>0$ would have worked for any angle of waveguide in $x<0$, not just the $\theta_0=0$ case that they envisaged. This is evidently because their coordinate transformation was applied to $x>0$ with no information about the geometry in $x<0$.

As discussed in Section 3, Berraquero *et al.* (2013) used a wide-spacing homogenisation for the structured bed which is not appropriate for the scale of their experiments. We have computed results for their configuration using the more appropriate close-spacing shallow-water homogenisation developed here. For example, in their third case of a bend of 30°, with their parameters $h^+=3.225h_0$, $h^-=0.310h_0$, $\delta=-53.05^\circ$ and $\Theta=0.5$ we find that $\theta_1=29.43^\circ$ and $|T|=0.946$. This is remarkably close to their intended design of $\theta_1=30^\circ$ and $|T|=1$ and helps explains why their results were so impressive. Using (4.20) with the bend design of $\theta_1=30^\circ$ and adopting their parameters $\delta=-53.05^\circ$, $\Theta=0.5$ predicts that the revised values of $h^+=2.636h_0$ and $h^-=0.232h_0$ would result in perfect transmission.

(a) Scattering by a structured bed of finite width

Consider now that the structured bed is confined to a strip of finite width $0<x<L$, $-\infty<y<\infty$ with a conventional fluid depth h_0 in $x<0$ and $x>L$. A wave is obliquely incident from $x<0$ making an angle θ_0 with the positive x-axis as before. The solution in $x<0$ is (4.6) whilst in $x>L$ the solution is

$$\eta(x,y)=T\mathrm{e}^{\mathrm{i}\alpha_0 x}\mathrm{e}^{\mathrm{i}\beta_0 y} \tag{4.21}$$

where T is the transmission coefficient. In $0<x<L$ the general solution is

$$\eta(x,y)=(A\mathrm{e}^{\mathrm{i}\alpha_1^+ x}+B\mathrm{e}^{\mathrm{i}\alpha_1^- x})\mathrm{e}^{\mathrm{i}\beta_0 y} \tag{4.22}$$

where the two wave components propagate flux/energy at angles $\pm\theta_1$ as determined from the direction of $\mathbf{c}_g$ in (4.15). Matching η and fluxes across $x=0$ and $x=L$ determines the solution. We find, after some routine algebra, that

$$R=\frac{((\alpha_0h_0)^2-Q^2)\sin(QL/\mathsf{h}_{11})}{((\alpha_0h_0)^2+Q^2)\sin(QL/\mathsf{h}_{11})+2\mathrm{i}\alpha_0h_0Q\cos(QL/\mathsf{h}_{11})} \tag{4.23}$$

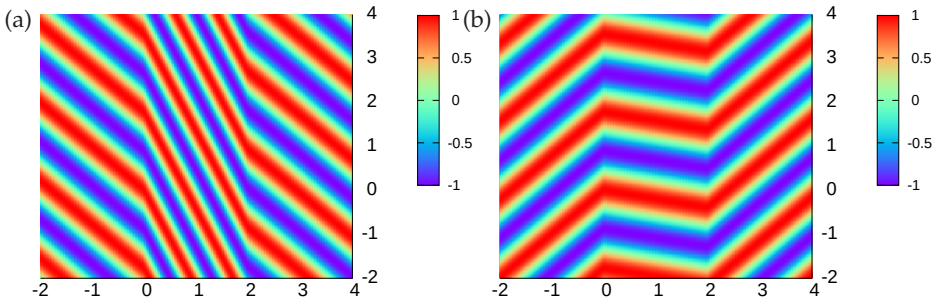

Figure 7. Instantaneous free surface plot on axes $(x/h_0, y/h_0)$ for a structured bed with $L/h_0 = 2$, for $\delta = 45^\circ$, $\Theta = 0$ at wavenumber $k_0 h_0 = 5$: (a) $h^+/h_0 = 1$, $h_0/h^- = 4$ and $\theta_0 = 45^\circ$; (b) $h_0/h^- = 1$, $h^+/h_0 = 4$ and $\theta_0 = -45^\circ$.

and A, B, T are also determined explicitly. We see that $R = 0$ either when $Q = \alpha_0 h_0$ or when $QL/\mathsf{h}_{11} = n\pi$, n an integer. Unsurprisingly the first of these is the same condition as for total transmission and zero reflection across a single interface – see equation (4.11). The second condition is a common multiple interference effect.

We can also consider wave trapping above the structured bed by considering $\beta_0 > k_0$ as a long-shore wavenumber independent from k_0 in the absence of an incident wave field. In doing so, waves in $x < 0$ and $x > L$ are evanescent and we assume parameters in $0 < x < L$ are chosen such that $\alpha_1^{\pm}$ are real (so that Q is real) implying waves over the structured bed. Matching general solutions across $x = 0$ and $x = L$ as above leads us to the condition for trapped waves of

$$\tan(QL/\mathsf{h}_{11}) = \frac{2\gamma_0 h_0 Q}{Q^2 - (\gamma_0 h_0)^2} \tag{4.24}$$

with $\gamma_0 = \sqrt{\beta_0^2 - k_0^2}$ and Q defined by (4.12). The only requirement for (4.24) to have solutions $\beta_0(k_0)$, apart from $\beta_0 > k_0$, is that Q is real.

Trapped modes are known to exist for raised rectangular steps of finite width (e.g. Mei (1983)) and were also found in Porter (2021) for tilted plate arrays of finite width extending through a constant depth fluid.

In Fig. 7 we have illustrated surface plots for scattering over a structured bed of finite extent with $L/h_0 = 2$ at wavenumber $k_0 h_0 = 5$ chosen for illustrative purposes (shallow water demands $k_0 h_0 \ll 1$). In both sub plots $\delta = 45^\circ$ and $\Theta = 0$. In the left-hand panel $h^+ = h_0$ and thin barriers protrude above the depth h_0 to a value of $h_0/h^- = 4$. The incident wave angle is $\theta_0 = 45^\circ$ and we know that there is perfect transmission across the bed and, from the results in Fig. 6 we have $\theta_1 \approx -11.3^\circ$ implying negative refraction. In the right-hand panel, $h^- = h_0$ and the thin barriers sit on a sunken level of $h^+/h_0 = 4$ with their tops level with h_0. The incident wave angle here is $\theta_0 = -45^\circ$ which also gives perfect transmission due to the symmetry of R with respect to θ_0 and the fact that an incident wave with $\theta_0 = 45^\circ$ does not feel a change in depths over the structured bed. In this example, $\theta_1 \approx -65^\circ$.

In Fig. 8 we present an instantaneous surface plot for a structured bed of width $L/h_0 = 2$ having the properties $\delta = 30^\circ$, $h_0/h^- = 3$, $h^+/h_0 = 3$ and with wavenumber $k_0 h_0 = 8$. To highlight the refractive features of the beds, a Gaussian beam is incident from $x < 0$ centred around three different incident wave angles, -50°, 0° and 50°. The structured bed corresponds to the case highlighted in Fig. 6 in which perfect transmission across the bed and into $x > L$ occurs across all wave angles. Since the Gaussian beam is formed by integrating incident over all wave angles with respect to Gaussian weight function centred on the principal wave heading we observe no reflection from the boundaries. In each sub-plot of Fig. 8 we observe varying degrees of negative refraction over the structured bed manifested as a shift in wave fronts as they pass from $x < 0$ to $x > L$. Fig. 8(a) provides us with an example of in which the x-component of the

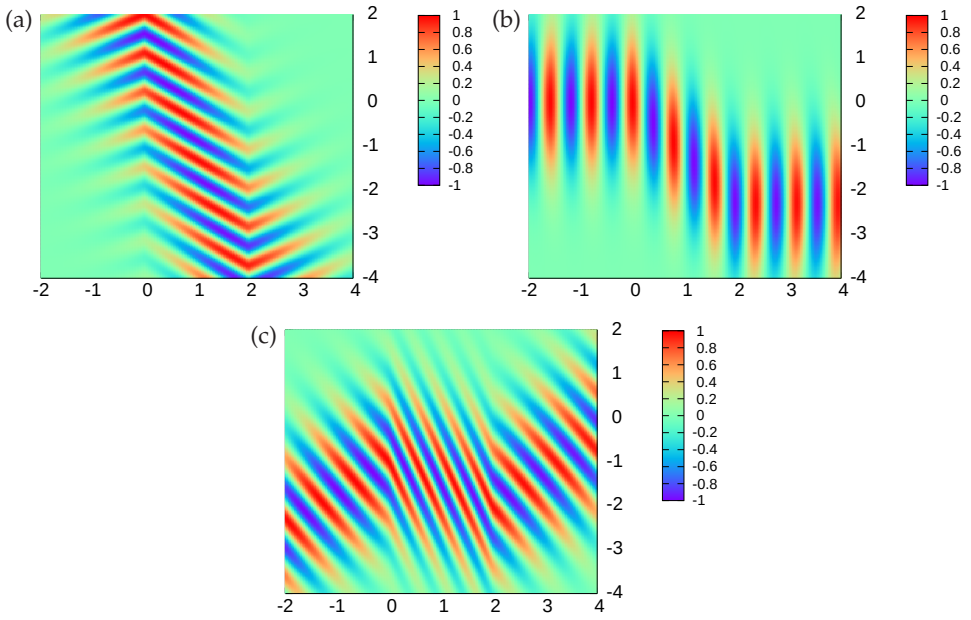

Figure 8. Instantaneous free surface plot on axes $(x/h_0, y/h_0)$ for a structured bed defined by $\delta = 30°$, $\Theta = 0$, $h^+/h_0 = 3$, $h_0/h^- = 3$ $L/h_0 = 2$ at wavenumber $k_0 h_0 = 8$ under a Gaussian beam centred around the incident wave angle $\theta_0 = -50°, \theta_0 = 0°, \theta_0 = 50°$.

phase velocity of both waves over the structured bed are negative (the direction of the phase velocity of the two wave modes are $-107°$ and $-153°$ with respect to the positive x-axis).

5. Propagating waves in curved channels

In this example, a more complex structured bed is used to propagate water waves through curved channels without reflection and retaining uniform wave crests. In related problems in acoustics and electromagnetics, see Han & Tang (2018) who proposed the use of a locally resonant metamaterial to propagate waves through curved channels without reflection.

Consider an infinitely-long waveguide of constant depth h_0 with walls along $y = a$ and $y = b$ for $-\infty < x < \infty$. Under the shallow water description of fluid motion, the surface elevation $\zeta(x, y, t)$ satisfies (1.1) with $\zeta_y = 0$ on $y = a$ and $y = b$, representing no flux normal to the walls. Waves propagate at the shallow water phase speed $c_0 = \sqrt{gh_0}$.

Now consider the mapping from (x, y) to (r, θ) defined by

$$x = L\theta/\alpha, \qquad y = a + (r^2 - a^2)/(b + a). \tag{5.1}$$

from the rectangular domain $0 < x < L$, $a < y < b$ to the annular domain $a < r < b$, $0 < \theta < \alpha$. Under this mapping, $\tilde{\zeta}(r, \theta, t) = \zeta(x, y, t)$, satisfies

$$\frac{1}{r}\frac{\partial}{\partial r}\left(rh_1\frac{\partial\tilde{\zeta}}{\partial r}\right) + \frac{1}{r}\frac{\partial}{\partial\theta}\left(\frac{h_2}{r}\frac{\partial\tilde{\zeta}}{\partial\theta}\right) = \frac{1}{g}\tilde{\zeta}_{tt} \tag{5.2}$$

provided we define

$$h_1(r) = h_0\frac{(b+a)^2}{4r^2}, \qquad h_2(r) = h_0\frac{\alpha^2 r^2}{L^2}. \tag{5.3}$$

In addition, $\tilde{\zeta}_r = 0$ on $r = a, b$.

Thus (5.2) is also a shallow water equation since, expressed in polar coordinates, we have

$$g\nabla\cdot(\mathsf{h}\nabla\tilde{\zeta})=\tilde{\zeta}_{tt}. \tag{5.4}$$

where $\mathsf{h}=\mathrm{diag}\{h_1,h_2\}$ represent effective depths experienced by waves propagating in radial and tangential directions (respectively). There are two possible structured bed configurations to choose from: corrugations in the bed can be aligned to $\hat{\mathbf{r}}$, the radial direction or $\hat{\boldsymbol{\theta}}$, the tangential direction. We imagine here that the bathymetry has radially-aligned corrugations and $h_1=h^-(r)$ represents the depth below the surface of the protrusions which decrease from a value $\frac{1}{4}h_0(b+a)^2/a^2$ at the inner wall to $\frac{1}{4}h_0(b+a)^2/b^2$ at the outer wall. Then $h_2=h^+(r)$ (taking $\Theta=0$ for simplicity) is the depth of the troughs between thin protruding barriers which increases from a value α^2a^2/L^2 to α^2b^2/L^2 across the width of the channel.

Although depths $h^+(r)$ and $h^-(r)$ can technically overlap within $a<r<b$ provided the orientation of the corrugations is reversed, it is easier to imagine this does not happen and this requires that $L<2\alpha a^2/(b+a)$ be satisfied.

The mapping can be used to consider two different problems. First, by letting $\alpha=2\pi$ we can consider waves propagating in an annular waveguide of inner radius a and outer radius b provided we ensure periodicity by setting $k_0L=2\pi m$ for m a positive integer. The solution is $\tilde{\zeta}(r,\theta,t)=\cos(k_0L\theta/2\pi-\omega t)$ and the amplitude, being independent of radius. Note, however, that this solution does not require a structured bed and can be realised under a conventional shallow water bed depth of $h(r,\theta)=h_0\alpha^2r^2/L^2$. In either case, the solution is distinct from waves propagating in a annular waveguide with a constant fluid depth h_0 where amplitudes depend on the radius being related to Bessel functions of argument k_0r.

Secondly, we can consider the reflection and transmission of incident waves propagating along a straight waveguide at the junction with a curved waveguide.

Writing $\zeta(x,y,t)=\Re\{\eta(x,y)\mathrm{e}^{-\mathrm{i}\omega t}\}$, the general solution to (1.1) in $x<0$ subject to the channel wall conditions and incorporating a plane wave incident from minus infinity is

$$\eta(x,y)=\mathrm{e}^{\mathrm{i}k_0x}+\sum_{n=0}^{\infty}R_n\mathrm{e}^{-\mathrm{i}\kappa_nx}\cos(n\pi(y-a)/(b-a)) \tag{5.5}$$

where $\kappa_n=\sqrt{k_0^2-(n\pi/(b-a))^2}=\mathrm{i}\sqrt{(n\pi/(b-a))^2-k_0^2}$ and R_n are amplitudes of reflected waves, either propagating (i.e. "cut-on" modes) or evanescent (i.e. "cut-off" modes) depending on wavenumber. In the curved guide, again with $\tilde{\zeta}(r,\theta,t)=\Re\{\tilde{\eta}(r,\theta)\mathrm{e}^{-\mathrm{i}\omega t}\}$, the general solution of (5.2) subject to Neumann conditions on $r=a$, $r=b$ is

$$\tilde{\eta}(r,\theta)=\sum_{n=0}^{\infty}T_n\mathrm{e}^{\mathrm{i}L\kappa_n\theta/\alpha}\cos(n\pi(r^2-a^2)/(b^2-a^2)). \tag{5.6}$$

By design, the expansion in (5.6) overlaps with (5.5) under the mapping (5.1). We have written (5.6) assuming that the curved guide extends indefinitely and waves are transmitted with transmission coefficients T_n as θ increases with no reflections returning from further up-wave junctions. The two solutions must be matched along the single fluid interface at $x=0^-$, $\theta=0^+$ for $a<r<b$ and upon which $r=y$. The leading order matching conditions from conventional bed depth h_0 in $x<0$ to the structured bed in $\theta>0$ are that pressure and flux are continuous and this provides us with

$$\eta(0^-,y)=\tilde{\eta}(y,0^+),\qquad h_0\eta_x(0^-,y)=\frac{h_2(y)}{y}\tilde{\eta}_\theta(y,0^+),\qquad a<y<b. \tag{5.7}$$

The non-linear nature of the mapping between r and y in (5.1) means that solutions are not perfectly matched without reflection by (5.7). Applying (5.7) to (5.5) and (5.6) using orthogonality the eigenfunctions in $x<0$ gives rise to the system of equations

$$\sum_{n=0}^{\infty}T_n(K_{mn}+L_{mn})=2\delta_{m0} \tag{5.8}$$

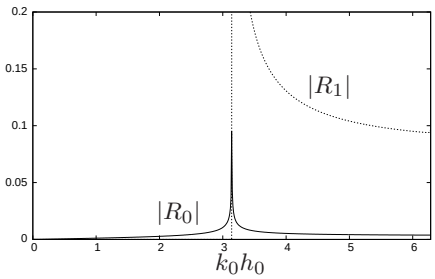

Figure 9. Reflection coefficients against wavenumber for scattering at the junction between straight and curved channels $a/h_0 = 2$, $b/h_0 = 3$ which under average impedance matching condition $\alpha a/L = 0.8$.

with $\delta_{m0} = 1$ for $m = 0$ and zero otherwise, wherein

$$R_m = -\delta_{m0} + \sum_{n=0}^{\infty} T_n K_{mn} \tag{5.9}$$

and where

$$K_{mn} = \epsilon_m \int_0^1 \cos(m\pi t)\cos(n\pi t(2a + (b-a)t)/(b+a))\, dt \tag{5.10}$$

$$L_{mn} = \frac{\kappa_n}{\kappa_m}\frac{\alpha\epsilon_m}{L}\int_0^1 (a + (b-a)t)\cos(m\pi t)\cos(n\pi t(2a + (b-a)t)/(b+a))\, dt \tag{5.11}$$

with $\epsilon_0 = 1$, $\epsilon_m = 2$ for $m = 1, 2, \ldots$. For $k_0 < \pi/(b-a)$ only one cut-on mode propagates in the channel and conservation of energy flux gives rise to the relation

$$|R_0|^2 + \frac{1}{2}\frac{\alpha}{L}(b+a)|T_0|^2 = 1. \tag{5.12}$$

For larger values of k_0 a revised energy equation can be established and is used as a check on the accuracy of numerical solutions Numerically, energy conservation was found to be satisfied to within 10^{-9} after truncation of (5.8) and (5.9) to fifty terms.

Although solutions cannot be perfectly impedance matched point-wise across $x = \theta = 0$, $a < r = y < b$, we can consider an impedance condition which arises from matching the flux averaged across the width of the channel and gives us

$$\frac{1}{2}\frac{\alpha}{L}(b+a) = 1. \tag{5.13}$$

This places a condition on the otherwise arbitrary dimensionless factor $\alpha a/L$ which encodes the stretching of the linear x-coordinate into the circular θ-coordinate in the curved guide.

In Fig. 9 we have imposed (5.13) and show the variation with k_0h_0 of $|R_0|$ and, for $k_0 > \pi/(b-a)$, $|R_1|$ in the case of $a/h_0 = 2$ and $b/h_0 = 3$. Prior to the first cut-on at $k_0h_0 = \pi$ there is very little reflected energy. In Fig. 10 we show the corresponding wave elevation for $k_0h_0 = 3$ in the case that (5.13) is satisfied (requiring $\alpha a/L = 0.8$) and for $\alpha a/L = 0.4$. In the first case $|R_0| = 0.0109$ and the wave propagates with no noticeable loss of form or reflection into the curved channel. In the second case, $|R_0| = 0.3378$, and there a more noticeable signature of reflection and a distortion of the wave field in the curved section due to imperfect impedance matching at the boundary.

For this problem supplementary calculations have shown that a structured bed is not necessary to guide incident plane waves from a straight-walled channel into a curved channel and that a conventional bed produces almost identical results. Thus, when $h_1 = h_2 = h_0\alpha^2 r^2/L^2$ the general

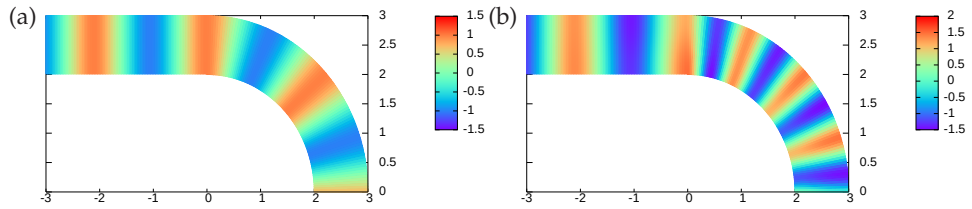

Figure 10. Instantaneous free surface plot on axes $(x/h_0, y/h_0)$ for waves under transition from a depth h_0 in $x<0$ to a structured bed in the bend for $a/h_0=2$, $b/h_0=3$ and $k_0h_0=3$ with: (a) $\alpha a/L=0.8$ and (b) $\alpha a/L=0.4$.

solution to (5.2) in the curved guide with $\tilde{\eta}_r=0$ on $r=a,b$ is, by separating variables,

$$\tilde{\eta}(r,\theta)=T_0\mathrm{e}^{\mathrm{i}k_0L\theta/\alpha}+\sum_{n=1}^{\infty}T_n\left(\frac{(r/b)^{\mathrm{i}\lambda_n-1}}{(\mathrm{i}\lambda_n-1)}-\frac{(r/b)^{-\mathrm{i}\lambda_n-1}}{(-\mathrm{i}\lambda_n-1)}\right)\mathrm{e}^{\mathrm{i}Ls_n\theta/\alpha} \tag{5.14}$$

where $\lambda_n=n\pi/\ln(a/b)$ and $s_n=\sqrt{k_0^2-\alpha^2(1+\lambda_n^2)/L^2}=\mathrm{i}\sqrt{\alpha^2(1+\lambda_n^2)/L^2-k_0^2}$. Matching to the general solution (5.5) via the conditions (5.7) in the same manner as previously described provides the solution here. A numerical and experimental study performed by Wang *et al.* (2015) used a similar device for bending waves through curved channels.

The study of curved channels with a fixed depth h_0 has a long history with analogues in acoustics and electromagnetics. Their solution via separation of variables is complicated – see the review article of Rostafinski (1991) – since the eigenvalues of the Sturm-Liouville system that arises determine the complex order of Bessel functions. A variety of approximations and computational methods have thus been devised to determine solutions to this problem (e.g. Felix & Pagneux (2001)). Because of this, we have not provided comparisons with propagation through a curved channel with constant depth h_0.

Although we've shown in the two problems here involving curved channels that structured bed are not necessary to engineer predetermined wave characteristics, there are examples where structured beds are essential. For instance, in the cloaking of cylinders as described by Zareei & Alam (2015) or as a wave rotator device as described by Chen *et al.* (2009).

6. Conclusion

In this paper we have provided a formal derivation based on multi-scale homogenisation of a shallow water theory for structured bathymetry comprised of rapidly-fluctuating corrugations. The model provides explicit expressions for the effective depth tensor components and complements existing models of Berraquero *et al.* (2013), which implicitly assumes wide-spacing between vertical protrusions and Maurel *et al.* (2017)'s semi-numerical scheme.

We have used the model to investigate and characterise the negative refraction of oblique plane waves propagating across the interface from conventional to structured bathymetry defined by spatially-constant effective depths. In doing so, we have shown that waves propagating energy away from the interface over the structured bathymetry can have a phase velocity directed towards the interface. We have also shown that there example of beds which are reflectionless for all incident wave angles and (under shallow water theory) frequencies, but which refract incident waves in a non-trivial way.

A demonstration of the use of spatially-varying effective depths is provided by an example involving engineering waves to propagate through curved channels without reflection or change in wave elevation.

This work could be a useful foundation to develop bathymetric devices for the protection of coastal assets such as harbours or for the bespoke manipulation of waves for ocean wave energy harnessing schemes.

Data Accessibility. Numerical code and data files for the results in this article are available to download from https://people.maths.bris.ac.uk/ marp/abstracts/metaswe.html.

Authors' Contributions. Both authors contributed equally to the development of the analysis and computation of numerical results. RP wrote the text.

Funding. CM is supported by an EPSRC Studentship number S139151-124

References

1. Berraquero, CP., Maurel, A., Petitjeans, P. Pagneux, V. 2013. Experimental realization of a water-wave metamaterial shifter. *Phys. Rev. E.* **88**, 051002.
2. Chen, H., Yang, J., Zi, J., Chan, CT. 2009. Transformation media for linear liquid surface waves. *EuroPhys. Lett.* **85**, 24004.
3. Farhat, M., Enoch, S., Guenneau, S., Movchan, A. 2008. Broadband cylindrical acoustic cloak for linear surface waves in a fluid. *Phys. Rev. Lett.* **101**, 134501.
4. Farhat, M., Guenneau, S., Enoch, S., Movchan, A. 2010. All-angle-negative-refraction and ultra-refraction for liquid surface waves in 2D phononic crystals. *J. Comp. Appl. Math.* **234**(6), 2011–2019.
5. Félix, S., Pagneux, V. 2001. Sound propagation in rigid bends: A multimodal approach. *J. Acoust. Soc. Am.* **110** 1329.
6. Fleury, R., Alù, A. 2014. Cloaking and Invisibility: A Review. *Progress In Electromagnetics Res.*, **147**, 171–20
7. Han, J., Tang, S. 2018. Realization of complex curved waveguide based on local resonant 3D metamaterial. *AIP Advances* **8**, 125327.
8. Iida, T., Kashiwagi, M. 2018. Small water channel network for designing wave fields in shallow water. *J. Fluid Mech.* **849**, 90–110.
9. Maurel, A., Marigo, J-J., Cobelli, P, Petitjeans, P., Pagneux, V. 2017. Revisiting the anisotropy of metamaterials for water waves. *Phys. Rev. B.* **96**, 134310.
10. Marigo, J-J., Maurel, A. 2017. Second order homogenization of subwavelength stratified media including finite size effect. *SIAM J. Appl. Math.* **77**(2), 721–743.
11. Mei, CC. 1983. *The Applied Dynamics of Ocean Surface Waves.* World Scientific.
12. Mei, CC., Vernescu, B. (2010) *Homogenization Methods for Multiscale Mechanics*. World Scientific.
13. Pendry, JB. 2000. Negative Refraction Makes a Perfect Lens. *Phys. Rev. Lett.* **85**, 3966.
14. Porter, R. 2018. Cloaking in water waves. In *Handbook of Metamaterials and Plasmonics, Vol. 2: Elastic, Acoustic, and Seismic Metamaterials* (Ed. S.A. Maier). World Scientific.
15. Porter, R. 2019. An extended linear shallow water equation. *J. Fluid Mech.* **876**, 413–427.
16. Porter, R. 2021. Plate arrays as water wave metamaterials. *Wave Motion* **100**, 102673.
17. Rosales, RR., Papanicolaou, GC. 1983. Gravity waves in a channel with a rough bottom. *Stud. Appl. Math.* **68**, 89–102.
18. Rostafinski, W. 1991. Monograph on propagation of sound waves in curved ducts. *NASA Reference Publ.* 1248.
19. Smith, DR., Pendry, JB., Wiltshire, MCK. 2004. Metamaterials and Negative Refractive Index. *Science* **305**(5685):788–92.
20. Stoker, JJ. 1957. *Water Waves*, Interscience, New York.
21. Wang, Z., Zhang, P., Nie, X., Zhang, Y. 2015. Manipulating water wave propagation via gradient index media. *Sci. Rep.* **5**, 16846.
22. Whitham, GB. 1974. *Linear and Nonlinear Waves.* Wiley-interscience, New York.
23. Zareei, A., Alam, M-R. 2015. Cloaking in shallow-water waves via nonlinear medium transformation. *J. Fluid Mech.* **778**, 273–287.
24. Zareei, A., Alam, M-R. 2016. Cloaking by a thin elastic plate. In *Proc. Int. Workshop on Water Waves and Floating Bodies, Michigan, USA.* Eds. Beck, R., Maki., K.